

Improved Green's Function Measurement for Hybridization Expansion Quantum Monte Carlo

Pavel Augustinský^{a,b,*}, Jan Kuneš^b

^a*Theoretical Physics III, Center for Electronic Correlations and Magnetism, Institute of Physics, University of Augsburg, D-86135, Augsburg, Germany*

^b*Institute of Physics, Czech Academy of Sciences, Cukrovarnická 10/112, 16200, Prague, Czech Republic*

Abstract

We present an algorithm for measurement of the Green's function in the hybridization expansion continuous-time quantum Monte-Carlo based on continuous estimators. Compared to the standard method, the present algorithm has similar or better accuracy with improvement notable especially at low perturbation orders and high frequencies. The resulting statistical noise is weakly correlated so high-accuracy data for the numerical analytical continuation can be produced.

Keywords: CT-HYB, Measurement

1. Introduction

The Monte-Carlo simulations are among the most widely used techniques for investigation of quantum impurity models. The progress of the dynamical mean-field theory [1, 2, 3] in the past decade, which allowed material specific studies of multi-band Hubbard models, is to a large extent governed by the availability of reliable and fast solvers for multi-orbital impurity problems. New generation quantum Monte-Carlo (QMC) techniques based on the stochastic sampling of perturbative expansions [4, 5, 6, 7] quickly became the standard of quantum impurity simulations.

Several QMC algorithms are currently used in this context differing by the type of expansion and symmetry of the impurity Hamiltonian. As the sim-

*Corresponding author

Email addresses: `august@fzu.cz` (Pavel Augustinský), `kunes@fzu.cz` (Jan Kuneš)

ulation of impurities with arbitrary interaction [8, 9] is computationally demanding, specialized algorithms that can handle a simplified density-density interaction at much lower computational cost still play an important role.

In this article we describe an improved technique for measurement of Green's functions in the strong-coupling CT-QMC algorithm (also called CT-HYB) for density-density interactions. The development was motivated by poor performance of the standard measurement technique in systems with strongly imbalanced perturbation orders for different orbitals. Such a situation is common in materials containing orbitals with fluctuating occupation coupled by interaction to filled or empty orbitals, e.g. the t_{2g} orbitals in nickelates [10], e_g orbitals in early transition metal oxides [11, 12], t_{2g} orbitals in the low-spin state of LaCoO_3 [13], or Hubbard model with crystal-field splitting [14, 15]. Although the filled orbitals experience little fluctuations themselves and their influence on the active (partially filled) orbitals is well approximated by a static potential, it is their Green's functions that may become prohibitively noisy. In some cases one can simply remove the filled orbitals from the effective model, e.g. early transition metals are commonly studied with t_{2g} -only models [16]. Often, however, some orbitals became filled/empty only in a certain part of the phase diagram and then they have to be kept in the model, e.g. to study spin/orbital ordering, or because one is interested in their dynamics, which may exhibit non-trivial dynamical renormalization [17, 10].

The paper is organized as follows. In section 2 we review the basic of the CT-HYB algorithm and the standard measurement technique. In section 3 we discuss on a general level the relationship between the expansions for the partition function and the Green's function. The new measurement algorithm is described in section 4 with details and implementation notes summarized in section 5. Finally, in section 6 we provide examples and performance tests.

2. CT-HYB

At this point, we briefly review the CT-HYB algorithm introduced in [4, 8] (for details see comprehensive review [7]).

We wish to study the dynamics of the d -electrons in the Anderson impurity model with *density-density* interaction described by the Hamiltonian

$$H = \sum_{\alpha k} \epsilon_{\alpha k} n_{\alpha k} + \sum_{\alpha} n_{\alpha} \left(E_{\alpha}^d + \sum_{\beta} U_{\alpha\beta} n_{\beta} \right) + \sum_{\alpha k} \left(V_{\alpha k} c_{\alpha k} d_{\alpha}^{\dagger} + h.c. \right) \quad (1)$$

consisting of three parts $H = H_{bath} + H_{loc} + H_{hyb}$. Bath fermionic operators are denoted by $c_{\alpha k}$, $c_{\alpha k}^\dagger$ while d_α , d_α^\dagger stand for the impurity operators and $n_\alpha = d_\alpha^\dagger d_\alpha$ are the corresponding occupation number operators. The flavor index α represents both the spin and the orbital quantum number. Our aim is to evaluate the Green's function

$$G_\alpha(\tau', \tau'') = -\langle T d_\alpha(\tau'') d_\alpha^\dagger(\tau') \rangle. \quad (2)$$

We assume the bath and the Green's function to be diagonal in the flavor indices throughout the paper but generalization to non-diagonal baths is possible.

The CT-HYB algorithm is based on the expansion of the partition function in the hybridization strength

$$\begin{aligned} Z &= \text{Tr} [e^{-\beta H}] = \text{Tr} \left[e^{-\beta(H_{bath} + H_{loc})} T e^{-\int_0^\beta H_{hyb}(\tau) d\tau} \right] = \\ &= \sum_{k=0}^{\infty} (-1)^k \int_0^\beta d\tau_1 \dots \int_{\tau_{k-1}}^\beta d\tau_k \text{Tr} [e^{-\beta(H_{bath} + H_{loc})} H_{hyb}(\tau_k) \dots H_{hyb}(\tau_1)]. \end{aligned} \quad (3)$$

For H_{loc} diagonal in the occupation number basis, expansion (3) can be viewed as a sum over so called *segment configurations* (Z -configurations). In a schematic way, it can be written as

$$Z = Z_{bath} \oint d\boldsymbol{\tau} Z(\boldsymbol{\tau}) = Z_{bath} \oint d\boldsymbol{\tau} Z_{loc}(\boldsymbol{\tau}) Z_{hyb}(\boldsymbol{\tau}), \quad (4)$$

The partition function of the bath Z_{bath} presents only an irrelevant multiplication factor. The abbreviation $\boldsymbol{\tau} \equiv \{\{\tau_i^s, \tau_i^e\}_\alpha\}$ is used here to describe all the integration variables, that is a set of start-times and end-times for all flavors. We stress that we use symbol $\boldsymbol{\tau}$ to describe an *arbitrary* set of numbers τ_i^s and τ_i^e from interval $(0, \beta)$. If $\boldsymbol{\tau}$ does not represent an allowed Z -configuration, $Z(\boldsymbol{\tau})$ is zero. Otherwise, we have

$$\begin{aligned} Z_{loc} &= \exp \left(- \sum n_\alpha E_\alpha^d - \sum_{\alpha < \beta} U_{\alpha\beta} o_{\alpha\beta} \right), \\ Z_{hyb} &= \prod_\alpha \det F_\alpha(\tau_i^e - \tau_j^s). \end{aligned} \quad (5)$$

where n_α and $o_{\alpha\beta}$ stand for the total length of segments of flavor α and their overlap with segments of flavor β , and $F_\alpha(\tau)$ is the hybridization function.

A random series of Z -configurations is generated using the Metropolis importance sampling with the probability density $Z(\boldsymbol{\tau})$. This series is then used to obtain various quantities of interest such as the Green's function (2). In the standard approach, from each Z -configuration with K segments of flavor α one obtains an estimator of the Green's function that consist of K^2 delta-functions

$$G_\alpha(\tau', \tau'') = \left\langle \sum_{ij} M_{ij}^\alpha \delta(\tau' - \tau_i^s) \delta(\tau'' - \tau_j^e) \right\rangle_{\text{MC}}. \quad (6)$$

Here, M_{ij}^α stands for the matrix element of the inverse hybridization matrix of flavor α . With this approach, however, difficulties are encountered when the mean perturbation order of the simulation is low. In such a case, the estimator (6) consists of only a few δ -functions and a poor statistics results. Moreover, due to the discrete character of estimators, a significant statistical noise is observed in $G_\alpha(i\omega_n)$, and even worse in the selfenergy, at higher frequencies.

Recently, a substantial progress has been achieved in fixing these problems. The statistical noise in the selfenergy (and the two-particle Green's function) can be significantly suppressed when improved estimators based on the equation of motion are used [18]. Besides that, filtering out the stochastic noise using orthogonal polynomial representation can be used to further improve the results [19]. Nevertheless, neither of these methods can fully avoid the poor statistics at low perturbation orders.

3. Measurement of the Green's function

There is not a unique way to estimate the Green's function from the random series of Z -configurations. In fact, there is a substantial freedom in this procedure and expression (6) presents only one of the possibilities. In this section, we review the general logic of the measurement and establish notation used in the rest of the paper.

Perturbation expansion of the Green's function can be, similarly to series (3), written as

$$G_\alpha(\tau', \tau'') = \frac{1}{Z} \oint d\boldsymbol{\tau} G_\alpha(\tau', \tau''; \boldsymbol{\tau}) = \frac{1}{Z} \oint d\boldsymbol{\tau} G_{loc}(\tau', \tau''; \boldsymbol{\tau}) G_{hyb}(\boldsymbol{\tau}). \quad (7)$$

It can be represented as a sum over segment configurations with one pair of special start-time and end-time at τ' and τ'' (G -configurations). In CT-HYB, series (7) is integrated by the Monte-Carlo method with $Z(\boldsymbol{\tau})$ used as

the probability density for the importance sampling. Unless $\tau' = \tau''$, there are regions of the $\boldsymbol{\tau}$ -space where $Z(\boldsymbol{\tau})$ is identically zero while $G_\alpha(\tau', \tau''; \boldsymbol{\tau})$ is not. Therefore, $Z(\boldsymbol{\tau})$ can *not* be used to directly sample expansion (7). In the standard approach, to each G -configuration $\{\tau', \tau'', \boldsymbol{\tau}_1\}$ we assign *one* Z -configuration $\boldsymbol{\tau}_2$ so that if $G_\alpha(\tau', \tau''; \boldsymbol{\tau}_1)$ is non-zero, $Z(\boldsymbol{\tau}_2)$ is non-zero as well. Then, once $\boldsymbol{\tau}_2$ is visited during the random walk, $G_\alpha(\tau', \tau''; \boldsymbol{\tau}_1)/Z(\boldsymbol{\tau}_2)$ is accumulated as the estimator for $G_\alpha(\tau', \tau'')$. Drawback of this approach is that we obtain information about $G_\alpha(\tau', \tau'')$ only when τ' and τ'' correspond to one start-time and one end-time in the visited Z -configuration.

The standard measurement can be generalized when to each $G_\alpha(\tau', \tau''; \boldsymbol{\tau}_1)$ we assign a *set* of configurations $Z(\boldsymbol{\tau}_2)$ with some weight distribution $w(\tau', \tau'', \boldsymbol{\tau}_1, \boldsymbol{\tau}_2)$ and accumulate

$$w(\tau', \tau'', \boldsymbol{\tau}_1, \boldsymbol{\tau}_2) \frac{G_\alpha(\tau', \tau''; \boldsymbol{\tau}_1)}{Z(\boldsymbol{\tau}_2)} = w(\tau', \tau'', \boldsymbol{\tau}_1, \boldsymbol{\tau}_2) \frac{G_{loc}(\tau', \tau'', \boldsymbol{\tau}_1) G_{hyb}(\boldsymbol{\tau}_1)}{Z_{loc}(\boldsymbol{\tau}_2) Z_{hyb}(\boldsymbol{\tau}_2)} \quad (8)$$

when *any* $\boldsymbol{\tau}_2$ is visited. In principle, the weight function can be chosen arbitrarily as long as normalization condition

$$\int d\boldsymbol{\tau}_2 w(\tau', \tau'', \boldsymbol{\tau}_1, \boldsymbol{\tau}_2) = 1 \quad (9)$$

is fulfilled for each τ', τ'' and $\boldsymbol{\tau}_1$. However, for the sake of efficiency, $w(\tau', \tau'', \boldsymbol{\tau}_1, \boldsymbol{\tau}_2)$ should be non-zero only when it is cheap to evaluate ratio $G_\alpha(\tau', \tau''; \boldsymbol{\tau}_1)/Z(\boldsymbol{\tau}_2)$ in equation (8).

4. Improved measurement

Here, we introduce a choice of the weight function $w(\tau', \tau'', \boldsymbol{\tau}_1, \boldsymbol{\tau}_2)$ which constitutes the improved measurement. For a given Z -configuration, we assign a non-zero weight to a set of G -configurations generated by removing of a hybridization line followed by a shift of the lone $d_\alpha(\tau_j'')$, $d_\alpha^\dagger(\tau_j')$ operators to all positions consistent with the remaining segments. This way, from any Z -configuration (apart from the zeroth order of the perturbation theory) we obtain a non-zero contribution to $G_\alpha(\tau', \tau'')$ for all values of arguments so the estimator of the Green's function is a continuous function of the imaginary time.

In the following, we distinguish two types of G -configurations. Those where τ' can be shifted to τ'' without crossing a segment boundary will

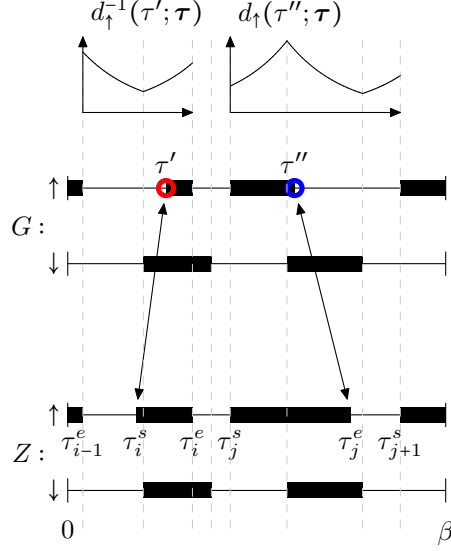


Figure 1: Relation between the separated G -configuration (top) and a Z -configuration (bottom). When we remove the hybridization line connecting τ_i^s and τ_j^e , we can reach G -configurations with $\tau'' \in (\tau_{i-1}^e, \tau_i^e)$ and $\tau' \in (\tau_j^s, \tau_{j+1}^s)$. The piecewise-exponential τ -dependence of functions $d_{\uparrow}(\tau; \tau)$ and $d_{\uparrow}^{-1}(\tau; \tau)$ is schematically depicted in the two graphs in the upper part of the figure. Regions with different atomic states are separated by the vertical dashed lines.

be called *connected*. Remaining ones will be called *separated*. The Green's function can be split into two terms corresponding to sums of series (7) over the connected and the separated configurations as

$$G_{\alpha}(\tau', \tau'') = G_{\alpha}^C(\tau', \tau'') + G_{\alpha}^S(\tau', \tau''). \quad (10)$$

Their evaluation is discussed in next two subsections.

4.1. Separated configurations

First, we discuss the evaluation of $G_{\alpha}^S(\tau', \tau'')$ which is somewhat simpler. In expression (8), the ratio of the bath traces equals the element of the inverse hybridization matrix as in the standard formula (6). The local traces differ by the position of one start-time and one end-time. At a fixed segment configuration, the local operators of flavor α “feel” an effective τ -dependent potential

$$E_{\alpha}^d(\tau; \tau) = E_{\alpha}^d + \sum_{\beta \neq \alpha} U_{\alpha\beta} n_{\beta}(\tau; \tau) \quad (11)$$

consisting of the site energy E_α^d and the interaction contribution due to all segments of other flavors. We define a function

$$d_\alpha(\tau; \boldsymbol{\tau}) = \exp\left(-\int_0^\tau d\sigma E_\alpha^d(\sigma; \boldsymbol{\tau})\right) \quad (12)$$

so that shifting of the creation operator from τ_i^s to τ' results in scaling the local trace by factor $d_\alpha(\tau_i^s; \boldsymbol{\tau})/d_\alpha(\tau'; \boldsymbol{\tau})$. When annihilation operator is moved from τ_j^e to τ'' , the local trace is scaled by $d_\alpha(\tau''; \boldsymbol{\tau})/d_\alpha(\tau_j^e; \boldsymbol{\tau})$. The lower bound of the integral in equation (12) can be chosen arbitrarily since it influences only an irrelevant multiplicative factor that cancels out. The estimator for the separated Green's function then reads

$$G_\alpha^S(\tau', \tau''; \boldsymbol{\tau}) = \sum_{\substack{ij \\ j \neq i, i+1}} M_{ij}^\alpha \frac{d_\alpha(\tau''; \boldsymbol{\tau}) d_\alpha(\tau_i^s; \boldsymbol{\tau})}{d_\alpha(\tau_j^e; \boldsymbol{\tau}) d_\alpha(\tau'; \boldsymbol{\tau})} w(\tau', \tau'', \tau_i^s, \tau_j^e; \boldsymbol{\tau}). \quad (13)$$

The summation does not include neighboring pairs of start- and end-times since they contribute to the connected part of the Green's function. We switched from abstract notation for weight $w(\tau', \tau'', \boldsymbol{\tau}_1, \boldsymbol{\tau}_2)$ and we explicitly indicate relevant imaginary-time arguments. In this notation, the normalization condition (9) reads

$$\int_{\tau_{i-1}^e}^{\tau_i^e} d\tau_i^s \int_{\tau_j^s}^{\tau_{j+1}^s} d\tau_j^e w(\tau', \tau'', \tau_i^s, \tau_j^e; \boldsymbol{\tau}) = 1. \quad (14)$$

So far, only the support of w was specified while its explicit functional form remains undetermined. In the following, we restrict ourselves to a factorized form

$$w(\tau', \tau'', \tau_i^s, \tau_j^e; \boldsymbol{\tau}) = w_c(\tau', \tau_i^s; \boldsymbol{\tau}) w_a(\tau'', \tau_j^e; \boldsymbol{\tau}). \quad (15)$$

The standard measurement formula (6) is restored with the δ -function weight $w_c = \delta(\tau'' - \tau_i^s)$, $w_a = \delta(\tau' - \tau_j^e)$. Since we want to improve on this and use the entire accessible imaginary-time interval, the uniform weight $w_c = 1/(\tau_i^e - \tau_{i-1}^e + \beta\theta(\tau_{i-1}^e - \tau_i^e))$, $w_a = 1/(\tau_{j+1}^s - \tau_j^s + \beta\theta(\tau_j^s - \tau_{j+1}^s))$ appears like a natural choice. However, our numerical experiments showed that it yields strong noise especially for strongly interacting systems and low temperatures

and it is always outperformed by the “normalization” weight

$$\begin{aligned}
w_c(\tau_i^s, \tau'; \boldsymbol{\tau}) &= d_\alpha^{-1}(\tau_i^s; \boldsymbol{\tau}) \left(\int_{\tau_{i-1}^e}^{\tau_i^e} d_\alpha^{-1}(\sigma; \boldsymbol{\tau}) d\sigma \right)^{-1} \chi_{(\tau_{i-1}^e, \tau_i^e)}(\tau'), \\
w_a(\tau_j^e, \tau''; \boldsymbol{\tau}) &= d_\alpha(\tau_j^e; \boldsymbol{\tau}) \left(\int_{\tau_j^s}^{\tau_{j+1}^s} d_\alpha(\sigma; \boldsymbol{\tau}) d\sigma \right)^{-1} \chi_{(\tau_j^s, \tau_{j+1}^s)}(\tau''). \quad (16)
\end{aligned}$$

Here, $\chi_{(a,b)}(\tau)$ stands for the characteristic function of interval (a,b) . With this weight, each δ -function of the standard formula (6) is smeared to a piecewise-exponential function with *unit* integral regardless of the initial position of τ_i^s and τ_j^e . This property makes the algorithm stable at any regime.

In principle, we can store estimator (13) in any basis during the simulation. Nevertheless, the imaginary time representation is inefficient because we must either introduce a large discretization error or use a fine imaginary-time grid which requires many numerically costly evaluations of expression (13). Despite its clear advantages, the recently proposed orthogonal polynomial representation for the Green’s function [19] is not well suited for our purpose either and we use the Matsubara basis. Its main advantage lies in the factorization property $\exp(i\omega_n(\tau' - \tau'')) = \exp(i\omega_n\tau') \exp(-i\omega_n\tau'')$ that reduces the computational complexity of the measurement. Besides that, it is simpler to Fourier transform a piecewise-exponential function than calculate its Legendre polynomial representation. In Matsubara frequencies with normalization weight (16) we obtain

$$\begin{aligned}
G_\alpha^S(i\omega_n) &= \frac{1}{\beta^2} \int_0^\beta \int_0^\beta d\tau' d\tau'' \exp(i\omega_n(\tau'' - \tau')) G_\alpha^S(\tau', \tau'') \\
&= \left\langle \sum_{\substack{ij \\ j \neq i, i+1}} M_{ij}^\alpha C_i^\alpha(i\omega_n) A_j^\alpha(i\omega_n) \right\rangle_{\text{MC}} \quad (17)
\end{aligned}$$

where functions $A_j^\alpha(i\omega_n)$ and $C_j^\alpha(i\omega_n)$ are given by

$$\begin{aligned}
A_j^\alpha(i\omega_n) &= \frac{1}{\beta} \int_{\tau_j^s}^{\tau_{j+1}^s} d\tau'' \frac{d_\alpha(\tau''; \boldsymbol{\tau})}{d_\alpha(\tau_j^e; \boldsymbol{\tau})} w_a(\tau_j^e, \tau''; \boldsymbol{\tau}) \exp(i\omega_n \tau'') = \frac{\tilde{A}_j^\alpha(i\omega_n)}{\tilde{A}_j^\alpha(0_+)}, \\
\tilde{A}_j^\alpha(i\omega_n) &= \frac{1}{\beta} \int_{\tau_j^s}^{\tau_{j+1}^s} d\tau'' d_\alpha(\tau''; \boldsymbol{\tau}) \exp(i\omega_n \tau''), \\
C_i^\alpha(i\omega_n) &= \frac{1}{\beta} \int_{\tau_{i-1}^e}^{\tau_i^e} d\tau' \frac{d_\alpha(\tau_i^s; \boldsymbol{\tau})}{d_\alpha(\tau'; \boldsymbol{\tau})} w_c(\tau_i^s, \tau'; \boldsymbol{\tau}) \exp(-i\omega_n \tau') = \frac{\tilde{C}_j^\alpha(i\omega_n)}{\tilde{C}_j^\alpha(0_+)}, \\
\tilde{C}_i^\alpha(i\omega_n) &= \frac{1}{\beta} \int_{\tau_{i-1}^e}^{\tau_i^e} d\tau' d_\alpha^{-1}(\tau'; \boldsymbol{\tau}) \exp(-i\omega_n \tau'). \tag{18}
\end{aligned}$$

In principle, the piecewise-exponential functions $d_\alpha(\tau'; \boldsymbol{\tau})$, $d_\alpha(\tau''; \boldsymbol{\tau})$ could be modulated by a to some extent arbitrary function if a τ', τ'' -dependent weight was chosen. However, the normalization condition (14) does not allow to chose the modulation independently for each τ_i^s , τ_j^e and this makes the choice of a better weight non-trivial. It remains an open question whether one can choose it in a more clever way so that it will, for instance, simplify numerical evaluation of equation (18).

4.2. Connected configurations

There are two different simple ways to reach a connected G -configuration from a Z -configuration. The first option is to remove a hybridization line spanning a single segment or antiselement and shift $d_\alpha(\tau'')$, $d_\alpha^\dagger(\tau')$ to a new position. The second option is to insert a $d_\alpha(\tau'')$, $d_\alpha^\dagger(\tau')$ pair into a Z -configuration. This approach is routinely used for estimation of the occupation numbers, that is the equal time Green's function. It can be used for measurement of the full Green's function for Hamiltonians including the spin-flip terms [6]. But for density-density interactions, the insertion measurement alone is not ergodic since it can not access the separated G -configurations. The two possibilities are shown in Figure 2 and we will discuss them separately.

4.2.1. "Remove and shift" approach

From the two types of G -configurations G_b and G_c depicted in Figure 2, we use a non-zero weight only for the later ones. Then, estimator for $G_\alpha^C(i\omega_n)$ is derived analogously to equation (13). The only difference here is that the

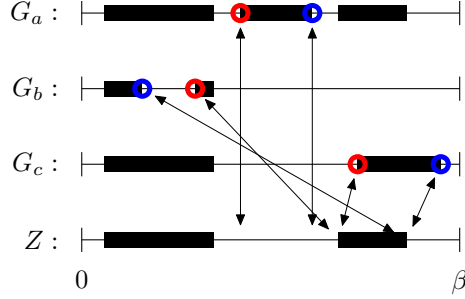


Figure 2: Different ways how a connected Green's function configuration can be reached from partition function configuration Z . G_a corresponds to insertion method. G_b and G_c can be obtained by removing of a hybridization line and shifting the remaining operators.

sum on the right hand side goes over complementary indices and τ' and τ'' must be properly ordered. In Matsubara frequencies we obtain

$$G_\alpha^C(i\omega_n) = \left\langle \sum_i M_{ii}^\alpha P_i^\alpha(i\omega_n) + M_{i+1,i}^\alpha H_i^\alpha(i\omega_n) \right\rangle_{\text{MC}} \quad (19)$$

where

$$\begin{aligned} P_i^\alpha(i\omega_n) &= \frac{1}{\beta^2} \int_{\tau_{i-1}^e}^{\tau_{i+1}^s} d\tau' \int_{\tau'}^{\tau_{i+1}^s} d\tau'' \frac{d_\alpha(\tau''; \boldsymbol{\tau})}{d_\alpha(\tau_j^e; \boldsymbol{\tau})} \frac{d_\alpha(\tau_i^s; \boldsymbol{\tau})}{d_\alpha(\tau'; \boldsymbol{\tau})} w(\tau_i^s, \tau_j^e, \tau', \tau''; \boldsymbol{\tau}) \exp(i\omega_n(\tau'' - \tau')), \\ H_i^\alpha(i\omega_n) &= -\frac{1}{\beta^2} \int_{\tau_i^s}^{\tau_{i+1}^e} d\tau' \int_{\tau_i^s}^{\tau'} d\tau'' \frac{d_\alpha(\tau''; \boldsymbol{\tau})}{d_\alpha(\tau_j^e; \boldsymbol{\tau})} \frac{d_\alpha(\tau_i^s; \boldsymbol{\tau})}{d_\alpha(\tau'; \boldsymbol{\tau})} w(\tau_i^s, \tau_j^e, \tau', \tau''; \boldsymbol{\tau}) \exp(i\omega_n(\tau'' - \tau')). \end{aligned} \quad (20)$$

Again, we can ensure the normalization with a weight function

$$w(\tau_i^s, \tau_j^e, \tau', \tau''; \boldsymbol{\tau}) = N \frac{d_\alpha(\tau_j^e; \boldsymbol{\tau})}{d_\alpha(\tau_i^s; \boldsymbol{\tau})} \quad (21)$$

where the multiplication factor N is chosen so that condition (9) is fulfilled. In the definition of $P_i^\alpha(i\omega_n)$ we have

$$\frac{1}{N} = \int_{\tau_{i-1}^e}^{\tau_{i+1}^s} d\tau_i^s \int_{\tau_i^s}^{\tau_{i+1}^e} d\tau_j^e \frac{d_\alpha(\tau_j^e; \boldsymbol{\tau})}{d_\alpha(\tau_i^s; \boldsymbol{\tau})} \quad (22)$$

and analogously for $H_i^\alpha(i\omega_n)$.

Individual estimators given by equation (19) do not have the exact $1/\omega$ asymptotic. Therefore, the stochastic noise in the Green's function decays with the inverse frequency and it is correlated. However, when apart from the Green's function we accumulate also the leading order coefficient in $G_\alpha^C(i\omega_n) \approx -iG_\alpha^\infty/\omega_n$, we can at the end of the simulation evaluate the Green's function as $G_\alpha^C(i\omega_n)/G_\alpha^\infty$. After this correction, the noise decays with the inverse *square* of frequency and its correlations are *suppressed*.

4.2.2. "Insertion" approach

With the insertion approach, there is only one Z -configuration from which a particular G -configuration can be created. Therefore, as in the standard measurement, the weight is uniquely determined by normalization condition (9). When there is at least one segment of flavor α , the estimator reads

$$G_\alpha^C(i\omega_n) = \left\langle \sum_i \tilde{P}_i^\alpha(i\omega_n) + \tilde{H}_i^\alpha(i\omega_n) \right\rangle_{\text{MC}}. \quad (23)$$

Unlike in equation (19), elements of the inverse hybridization matrix are missing here and definitions of $\tilde{P}_i^\alpha(i\omega_n)$ and $\tilde{H}_i^\alpha(i\omega_n)$ cover shorter imaginary-time intervals (corresponding to only one segment or antisection)

$$\begin{aligned} \tilde{P}_i^\alpha(i\omega_n) &= \frac{1}{\beta^2} \int_{\tau_i^s}^{\tau_i^e} d\tau' \int_{\tau_i^s}^{\tau'} d\tau'' \frac{d_\alpha(\tau''; \boldsymbol{\tau})}{d_\alpha(\tau'; \boldsymbol{\tau})} \exp(i\omega_n(\tau'' - \tau')), \\ \tilde{H}_i^\alpha(i\omega_n) &= -\frac{1}{\beta^2} \int_{\tau_i^e}^{\tau_{i+1}^s} d\tau' \int_{\tau'}^{\tau_{i+1}^s} d\tau'' \frac{d_\alpha(\tau''; \boldsymbol{\tau})}{d_\alpha(\tau'; \boldsymbol{\tau})} \exp(i\omega_n(\tau'' - \tau')). \end{aligned} \quad (24)$$

Unlike with the RS method, we obtain non-zero estimator $I_0^\alpha(i\omega_n)$ even from Z -configurations with no segments of flavor α . Then, there are only two possible states: the empty-line and the full-line. Given the configuration of other segments, probabilities of the two are given by $p_0 = 1/(1 + d_\alpha(\beta; \boldsymbol{\tau}))$ and $p_1 = d_\alpha(\beta; \boldsymbol{\tau})/(1 + d_\alpha(\beta; \boldsymbol{\tau}))$. We can use this and write

$$I_0^\alpha(i\omega_n) = \frac{1}{\beta^2} \frac{1}{1 + d_\alpha(\beta; \boldsymbol{\tau})} \int_0^\beta d\tau' \int_{\tau'}^{\tau'+\beta} d\tau'' \frac{d_\alpha(\tau''; \boldsymbol{\tau})}{d_\alpha(\tau'; \boldsymbol{\tau})} \exp(i\omega_n(\tau'' - \tau')). \quad (25)$$

This estimator is accumulated *regardless* of whether we reach the empty-line or the full-line state.

With the insertion method, each estimator obeys the exact $G_\alpha(i\omega_n) \rightarrow 1/i\omega_n$ asymptotic because the sum of lengths of all segments and antisections equals to β and estimator (25) is normalized by the probability prefactor. Therefore, the stochastic noise scales with ω^{-2} at high frequencies.

4.2.3. Comparison with RS method

When the mean perturbation order is very low, the insertion method is more accurate than the RS method since it works directly from the zeroth perturbation order. However, in most practical situations, it has ergodicity issues beyond the weak-coupling regime. In strongly interacting systems, segments of different flavors are typically anti-correlated so insertion method leads to inefficient importance sampling worsening exponentially with $U(\tau'' - \tau')$.

The best performance is delivered when we use a combination of the two approaches. At zeroth order, we use the insertion measurement since in this case ergodicity is assured by the probability factor in (25). For higher-order G -configurations we use the RS method. With this combination, there is no instability and poor statistics can occur only in the unlikely situation with the perturbation order sharply peaked around one. Further, when we refer to the RS method, this combination is implicitly assumed.

4.3. Selfenergy

Recently, an efficient estimator for the selfenergy in CT-HYB was proposed in [18]. The method is based on the observation that the selfenergy can be expressed from the equation of motion for the Green's function as

$$\Sigma_\alpha(i\omega_n) = \frac{F_\alpha(i\omega_n)}{G_\alpha(i\omega_n)} \quad (26)$$

where function $F_\alpha(i\omega_n)$ is the Fourier transform of the correlation function

$$F_\alpha(\tau' - \tau'') = - \sum_{\beta \neq \alpha} U_{\alpha\beta} \langle T d_\alpha(\tau') d_\alpha^\dagger(\tau'') n_\beta(\tau'') \rangle. \quad (27)$$

This method is superior to direct use of the Dyson equation since the selfenergy is calculated as a ratio of two quantities and only relative errors propagate. It can be naturally combined with the present measurement procedure. All we need to do in order to use estimator (26) is to measure the correlation function $F_\alpha(\tau' - \tau'')$. From the definition of the effective time-dependent atomic energy (11) we see that

$$\sum_{\beta \neq \alpha} U_{\alpha\beta} n_\beta(\tau; \boldsymbol{\tau}) = E_\alpha^d(\tau; \boldsymbol{\tau}) - E_\alpha^d \quad (28)$$

Therefore, regardless of what estimator $G_\alpha(\tau', \tau''; \boldsymbol{\tau})$ we use for the Green's function, the estimator for the F -function is given simply by

$$F_\alpha(\tau', \tau''; \boldsymbol{\tau}) = G_\alpha(\tau', \tau''; \boldsymbol{\tau}) (E_\alpha^d(\tau'; \boldsymbol{\tau}) - E_\alpha^d). \quad (29)$$

In comparison to measurement of the Green's function itself, this step is numerically cheap and requires only an acceptable overhead.

4.3.1. Dynamic part of the selfenergy

The selfenergy can be analytically continued to the real axis using the maximum-entropy method [20, 21] in the similar way as the Green's function. However, for the MAX-ENT method it is necessary that the continued function converges to zero for large frequencies. The full selfenergy does not fulfill this condition because of the constant Hartree-Fock term. Nevertheless, its dynamic part

$$\Sigma_{\alpha}^D(i\omega_n) = \Sigma_{\alpha}(i\omega_n) - \Sigma_{\alpha}^{\text{HF}} \quad (30)$$

does. So, in order to use the MAX-ENT analytical continuation, we have to measure the Hartree-Fock selfenergy separately and at the end of the simulation, we subtract it from the full selfenergy given by equation (26). We can further reduce error bars of the dynamic part when the estimator for $\Sigma_{\alpha}^{\text{HF}}$ is chosen so that it is correlated with asymptotic behavior of the full selfenergy. This is achieved by separate accumulating of the asymptotic leading order coefficients G_{α}^{∞} and F_{α}^{∞} and using their ratio as the estimator for $\Sigma_{\alpha}^{\text{HF}}$

$$\Sigma_{\alpha}^D(i\omega_n) = \frac{F_{\alpha}(i\omega_n)}{G_{\alpha}(i\omega_n)} - \frac{F_{\alpha}^{\infty}}{G_{\alpha}^{\infty}}. \quad (31)$$

The values of G_{α}^{∞} and F_{α}^{∞} depend only on the connected part of the Green's function and the F function

$$\begin{aligned} G_{\alpha}^{\infty} &= \frac{1}{\beta} \int_0^{\beta} d\tau G_{\alpha}^C(\tau_+, \tau) - G_{\alpha}^C(\tau_-, \tau), \\ F_{\alpha}^{\infty} &= \frac{1}{\beta} \int_0^{\beta} d\tau F_{\alpha}^C(\tau_+, \tau) - F_{\alpha}^C(\tau_-, \tau). \end{aligned} \quad (32)$$

For the insertion method, these equations reduce to simple expressions $G_{\alpha}^{\infty} = 1$ and $F_{\alpha}^{\infty} = \sum_{\beta \neq \alpha} U_{\alpha\beta} \langle n_{\beta} \rangle$ while for the remove-and-shift approach no such simplifications arise.

5. Implementation notes

In this section we summarize all steps necessary for implementation of the algorithm described above. We can provide full source code of our implementation upon email request.

First, at the beginning of the simulation, in order to avoid repeated computations of eigenvalues of the atomic Hamiltonian E_{loc} , we can store them into an array indexed by integer representing the local state (individual bits of the index can naturally represent occupation numbers of different flavors).

Next, given a Z configuration from the Metropolis random walk, we must divide the imaginary-time axis to regions with fixed atomic states. Each region is bounded by two hybridization events at τ_k and τ_{k+1} and has length $\Delta\tau_k = \tau_{k+1} - \tau_k$. For each τ_k and each Matsubara frequency we compute $\exp(i\omega_n\tau_k)$ and store it (the factorization property of exponential must be used in order to carry out this step efficiently).

Further, for each flavor α we calculate the effective local atomic energy $E_{\alpha k}^d$ from equation (11), exponential factors $\exp(-E_{\alpha k}^d\Delta\tau_k)$ and $d_\alpha(\tau_k; \boldsymbol{\tau}) = \prod_{l=0}^{k-1} \exp(-E_{\alpha l}^d\Delta\tau_l)$ defined by equation (12).

For each Matsubara frequency and each region (using the precomputed arrays), we calculate the following four quantities

$$\begin{aligned}
a_k^\alpha(i\omega_n) &= \int_{\tau_k}^{\tau_{k+1}} d\tau \exp(-E_{\alpha k}^d(\tau - \tau_k)) \exp(i\omega_n\tau) = \\
&\quad (\exp(-E_{\alpha k}^d\Delta\tau_k) \exp(i\omega_n\tau_{k+1}) - \exp(i\omega_n\tau_k)) / (i\omega_n - E_{\alpha k}^d), \\
c_k^\alpha(i\omega_n) &= \int_{\tau_k}^{\tau_{k+1}} d\tau \exp(E_{\alpha k}^d(\tau - \tau_k)) \exp(-i\omega_n\tau) = \\
&\quad (\exp(-i\omega_n\tau_k) - \exp(E_{\alpha k}^d\Delta\tau_k) \exp(-i\omega_n\tau_{k+1})) / (i\omega_n - E_{\alpha k}^d), \\
p_k^\alpha(i\omega_n) &= \frac{1}{\beta^2} \int_{\tau_k}^{\tau_{k+1}} d\tau' \int_{\tau'}^{\tau_{k+1}} d\tau'' \exp(E_{\alpha k}^d(\tau' - \tau'')) \exp(i\omega_n(\tau'' - \tau')), \\
&\quad (\exp((i\omega_n - E_{\alpha k}^d)\Delta\tau_k) - 1 - (i\omega_n - E_{\alpha k}^d)\Delta\tau_k) / (i\omega_n - E_{\alpha k}^d)^2 = \\
&\quad (a_k^\alpha(i\omega_n) \exp(-i\omega_n\tau_k) - \Delta\tau_k) / (i\omega_n - E_{\alpha k}^d), \\
h_k^\alpha(i\omega_n) &= -\frac{1}{\beta^2} \int_{\tau_k}^{\tau_{k+1}} d\tau' \int_{\tau_k}^{\tau'} d\tau'' \exp(E_{\alpha k}^d(\tau' - \tau'')) \exp(i\omega_n(\tau'' - \tau')) = \\
&\quad (1 - \exp(-(i\omega_n - E_{\alpha k}^d)\Delta\tau_k) - (i\omega_n - E_{\alpha k}^d)\Delta\tau_k) / (i\omega_n - E_{\alpha k}^d)^2 = \\
&\quad = (c_k^\alpha(i\omega_n) \exp(i\omega_n\tau_k) - \Delta\tau_k) / (i\omega_n - E_{\alpha k}^d). \tag{33}
\end{aligned}$$

From these quantities we build-up the functions $A_j^\alpha(i\omega_n)$, $C_j^\alpha(i\omega_n)$, $P_j^\alpha(i\omega_n)$ and $H_j^\alpha(i\omega_n)$ defined by equations (18) and (20). In order to use the weight given by equations (16) and (21), we also need to evaluate the corresponding normalization integrals that can be expressed in terms of zero-frequency limits $a_j^\alpha(0_+)$, $c_j^\alpha(0_+)$, $p_j^\alpha(0_+)$ and $h_j^\alpha(0_+)$. Unless $|E_{\alpha k}^d\Delta\tau_k| \ll 1$, we can calculate these values simply by putting $i\omega_n = 0$ in equations (33). Otherwise,

we must use the Taylor expansions

$$\begin{aligned}
a_k^\alpha(0) &= \Delta\tau_k - \frac{1}{2}E_{\alpha k}^d \Delta\tau_k^2 + \dots \\
c_k^\alpha(0) &= \Delta\tau_k + \frac{1}{2}E_{\alpha k}^d \Delta\tau_k^2 + \dots \\
p_k^\alpha(0) &= \frac{\Delta\tau_k^2}{2} - \frac{1}{6}E_{\alpha k}^d \Delta\tau_k^2 + \dots \\
h_k^\alpha(0) &= \frac{\Delta\tau_k^2}{2} + \frac{1}{6}E_{\alpha k}^d \Delta\tau_k^2 + \dots
\end{aligned} \tag{34}$$

Finally, we have

$$\begin{aligned}
\tilde{A}_i^\alpha(i\omega_n) &= \sum_{k=k_s}^{k_e} d_\alpha(\tau_k; \boldsymbol{\tau}) a_k^\alpha(i\omega_n), \text{ where : } \tau_{k_s} = \tau_i^s, \tau_{k_e+1} = \tau_{i+1}^s, \\
A_i^\alpha(i\omega_n) &= \frac{1}{\beta} \frac{\tilde{A}_i^\alpha(i\omega_n)}{\tilde{A}_i^\alpha(0_+)}, \\
\tilde{C}_i^\alpha(i\omega_n) &= \frac{1}{\beta} \sum_{k=k_s}^{k_e} d_\alpha^{-1}(\tau_k; \boldsymbol{\tau}) c_k^\alpha(i\omega_n), \text{ where : } \tau_{k_s} = \tau_{i-1}^e, \tau_{k_e+1} = \tau_i^e, \\
C_i^\alpha(i\omega_n) &= \frac{1}{\beta} \frac{\tilde{C}_i^\alpha(i\omega_n)}{\tilde{C}_i^\alpha(0_+)}, \\
\tilde{P}_i^\alpha(i\omega_n) &= \sum_{k=k_s}^{k_e} p_k^\alpha(i\omega_n) + \sum_{k=k_s}^{k_e-1} \sum_{l=k+1}^{k_e} \frac{d_\alpha(\tau_l; \boldsymbol{\tau})}{d_\alpha(\tau_k; \boldsymbol{\tau})} c_k^\alpha(i\omega_n) a_l^\alpha(i\omega_n), \\
&\text{where : } \tau_{k_s} = \tau_{i-1}^e, \tau_{k_e+1} = \tau_{i+1}^s, \\
P_i^\alpha(i\omega_n) &= \frac{1}{\beta^2} \frac{\tilde{P}_i^\alpha(i\omega_n)}{\tilde{P}_i^\alpha(0_+)}, \\
\tilde{H}_i^\alpha(i\omega_n) &= \sum_{k=k_s}^{k_e} h_k^\alpha(i\omega_n) + \sum_{k=k_s}^{k_e-1} \sum_{l=k+1}^{k_e} \frac{d_\alpha(\tau_k; \boldsymbol{\tau})}{d_\alpha(\tau_l; \boldsymbol{\tau})} a_k^\alpha(i\omega_n) c_l^\alpha(i\omega_n), \\
&\text{where : } \tau_{k_s} = \tau_i^s, \tau_{k_e+1} = \tau_{i+1}^e, \\
H_i^\alpha(i\omega_n) &= \frac{1}{\beta^2} \frac{\tilde{H}_i^\alpha(i\omega_n)}{\tilde{H}_i^\alpha(0_+)}.
\end{aligned} \tag{35}$$

Evaluation of the double sums in definitions of $\tilde{P}_i^\alpha(i\omega_n)$ and $\tilde{H}_i^\alpha(i\omega_n)$ can be accelerated when results from evaluation of $\tilde{A}_i^\alpha(i\omega_n)$ and $\tilde{C}_i^\alpha(i\omega_n)$ are reused and its cost is linear in number of covered regions $k_e - k_s$. The zeroth

order term (25) can be evaluated analogously, but order in which individual summations are carried out must be chosen based on sign of $d_\alpha(\beta; \tau) - 1$ in order to avoid the numerical instability. Finally, with results of equations (35), we can compute estimators (17) and (19).

5.1. Computational complexity

The obvious disadvantage of the algorithm described in this paper compared to the standard measurement is the increased computational cost. Unlike the standard approach, our measurement is causing a non-negligible slow-down of the entire simulation.

Overall, the computational complexity of the improved measurement scales *quadratically* with the perturbation order and linearly with the number of measured Matsubara frequencies because of evaluation of equation (17). Nevertheless, the standard estimator (6) has a similar form and it is not the real computational bottleneck for any reasonable perturbation order. In practice, the most expensive part of our algorithm is computation of the functions $A_j^\alpha(i\omega_n)$, $C_j^\alpha(i\omega_n)$, $P_j^\alpha(i\omega_n)$ and $H_j^\alpha(i\omega_n)$ from equation (35) (including all of its inputs). Its cost, however, is only *linear* in the total number of regions, Matsubara frequencies and flavors. Therefore, relative cost of measurement compared to one MC step is decreasing with increasing perturbation order (temperature). Nevertheless, it is essential not to perform measurement after every Monte-Carlo step but only approximately once the autocorrelation time to keep the simulation speed reasonable.

6. Results

In this section, we present the numerical results for two test cases. First, the single band Anderson impurity model with the semielliptic density of states (half band-width is set to one). Second, as an example of a realistic material calculation, we show results for the cobalt atom in LaCoO_3 . If not explicitly stated otherwise, we use the RS measurement. As a benchmark, results obtained with delta estimators measured to Matsubara frequencies and Legendre polynomials are used. Our implementation is based on the hybridization-expansion solver [22] from the ALPS library version 2 [23, 24]. All the other results shown here were also obtained using the ALPS library.

In figure 3, the impurity selfenergy for the half-filled Anderson model for $U = 1$ and $\beta = 10$ (mean perturbation order 1.8) is plotted. The results were obtained from the equation of motion (26) using independent simulations and

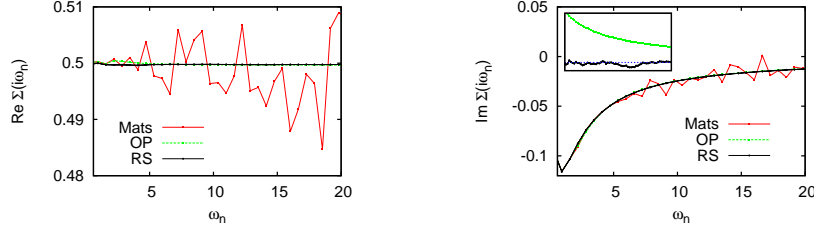


Figure 3: The real and the imaginary part of the selfenergy for $U = 1$ and $\beta = 10$. The red and the green line were obtained from delta estimators measured into Matsubara frequencies and Legendre polynomials. Inset in the right graph shows the difference between the measured selfenergy and the analytically computed high-frequency tail.

the same amount of CPU time. We intentionally use short MC runs here in order to make the statistical noise visible to the naked eye. While noise from the standard method is increasing with frequency, no such effect is visible when continuous estimators or measurement into orthogonal polynomials are used. With the orthogonal polynomials, however, the stochastic noise is suppressed at the price of introducing strong statistical correlations between the values at different Matsubara frequencies. Correlations in the imaginary part of the selfenergy obtained from the RS method are much weaker. This is demonstrated in the inset which shows the difference between the measured selfenergy and the analytically computed high-frequency tail. Errors of the real part of the selfenergy are strongly correlated because of uncertainty in the Hartree-Fock term. These correlations can be eliminated in the dynamic selfenergy by means of equation (31).

Next, we show comparison of accuracies of different methods in figure 4. We plot the relative error, that is, the ratio of the errors obtained with continuous estimators and the error from the standard formula. The comparison between the insertion method and the RS method shows that while the first one has better high-frequency behavior, it is (exponentially) unstable in the strong coupling regime. On the contrary, the RS method yields more accurate results regardless of U . The temperature dependence of the relative error from the RS measurement shows that benefits of this approach persist even in higher perturbation orders. The correction on the exact $1/\omega$ asymptotic discussed in section 4.2.1 further increases the accuracy.

In figure 5, the selfenergy of lanthanum cobaltite is plotted. The impurity

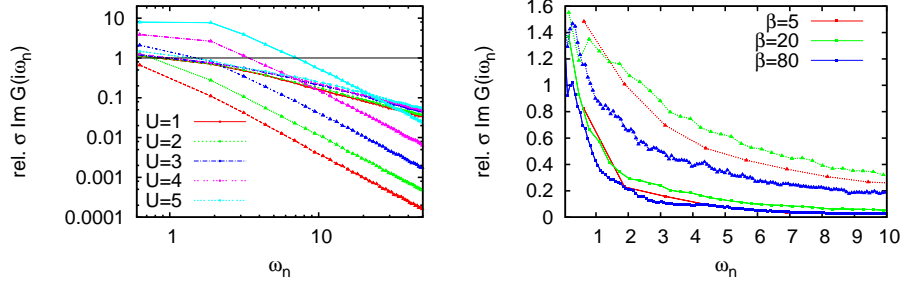


Figure 4: Left: Comparison of relative error bars of the imaginary part of the Green's function for $U = 1, 2, 3, 4$ and 5 and $\beta = 5$. Errors from the insertion approach (labeled with triangles) are lower in the weak-coupling regime, but they grow exponentially with increasing interaction. On the contrary, the RS measurement (labeled with circles) yields almost interaction-independent results. Right: Relative errors for $U = 1$ and different temperatures with (squares) and without (triangles) the correction on the correct asymptotic behavior. The mean perturbation order here grows approximately linearly with temperature up to $\langle K \rangle \approx 16$ at $\beta = 80$.

model used describes the full d-shell of cobalt with five orbitals. The perturbation order is strongly imbalanced here. While the mean perturbation order of t_{2g} orbitals is very low, $\langle K \rangle \approx 0.3$, e_g orbitals are strongly hybridized with $\langle K \rangle \approx 42$. The e_g selfenergy measured with the RS method is less accurate than the one obtained from the standard formula apart from the high-frequency tail. The reason for this is that the same amount of CPU time was used for both simulations and only approximately 60% of Monte Carlo steps were done with the slower RS method.

7. Conclusions and outlook

The presented measurement algorithm for the Green's function has several possible applications. First of all, it solves the poor statistics problem at low perturbation orders. At higher orders, it yields stochastic noise decreasing with Matsubara frequency so it can generate better data for the numerical analytical continuation of both the Green's function and the selfenergy. In principle, it also allows for measurement of a general local susceptibility of non density-density type that is very difficult to obtain with the standard method.

Its main disadvantage is relatively high computational complexity resulting in slowdown of the entire simulation and slightly worse accuracy at low

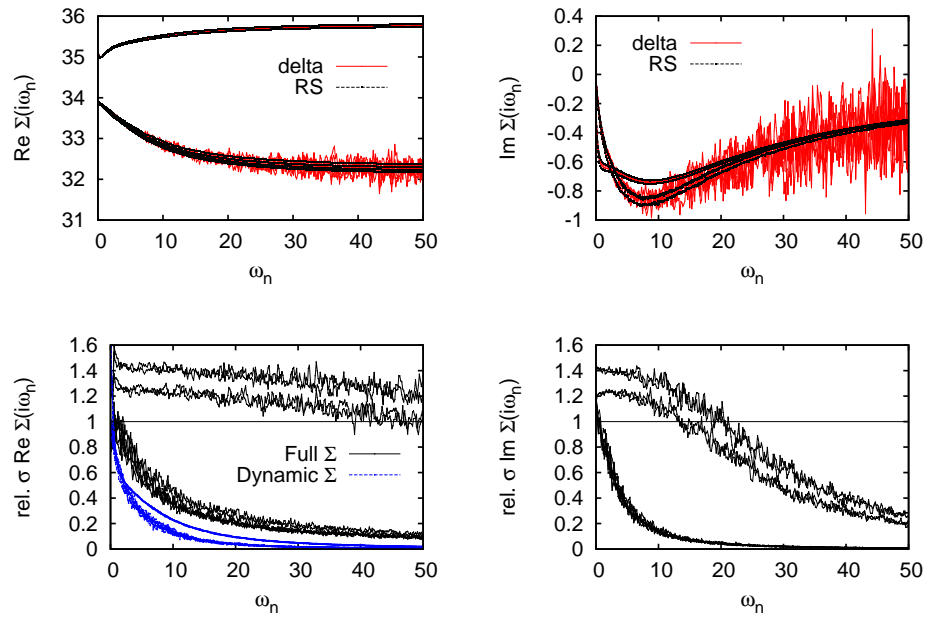


Figure 5: Top: The selfenergy of lanthanum cobaltite calculated with delta estimators and the RS method. The two branches correspond to the weakly hybridized t_{2g} orbitals and the strongly hybridized e_g orbitals. Bottom: Relative errors of the full selfenergy and its dynamic part.

frequencies. Moreover, since our method essentially relies on fast and simple evaluation of the local trace, generalization to the matrix formalism would be difficult, if possible at all.

8. Acknowledgement

We acknowledge inspiring discussions with Marcus Kollar, Liviu Chioncel and Junya Otsuki during development of this method. The research on this project was supported by Deutsche Forschungsgemeinschaft Research Unit FOR 1346. All calculations were done on the Dorje cluster at the Institute of Physics of the Czech Academy of Sciences in Prague.

References

- [1] A. Georges, G. Kotliar, W. Krauth, M. J. Rozenberg, *Rev. Mod. Phys.* 68 (1) (1996) 13.
- [2] K. Held, I. A. Nekrasov, G. Keller, V. Eyert, N. Blümer, A. K. McMah-an, R. T. Scalettar, T. Pruschke, V. I. Anisimov, D. Vollhardt, *phys. stat. sol. (b)* 243 (2006) 2599.
- [3] G. Kotliar, S. Y. Savrasov, K. Haule, V. S. Oudovenko, O. Parcollet, C. A. Marianetti, *Rev. Mod. Phys.* 78 (2006) 865.
- [4] P. Werner, A. Comanac, L. de’ Medici, M. Troyer, A. J. Millis, *Phys. Rev. Lett.* 97 (2006) 076405.
- [5] A. N. Rubtsov, V. V. Savkin, A. I. Lichtenstein, *Phys. Rev. B* 72 (2005) 035122.
- [6] K. Haule, *Phys. Rev. B* 75 (2007) 155113.
- [7] E. Gull, A. J. Millis, A. I. Lichtenstein, A. N. Rubtsov, M. Troyer, P. Werner, *Rev. Mod. Phys.* 83 (2011) 349–404.
- [8] P. Werner, A. J. Millis, *Phys. Rev. B* 74 (2006) 155107.
- [9] A. M. Läuchli, P. Werner, *Phys. Rev. B* 80 (2009) 235117.
- [10] X. Deng, M. Ferrero, J. Mravlje, M. Aichhorn, A. Georges, *Phys. Rev. B* 85 (2012) 125137.

- [11] K. Held, G. Keller, V. Eyert, D. Vollhardt, V. I. Anisimov, Phys. Rev. Lett. 86 (2001) 5345–5348.
- [12] I. A. Nekrasov, G. Keller, D. E. Kondakov, A. V. Kozhevnikov, T. Pruschke, K. Held, D. Vollhardt, V. I. Anisimov, Phys. Rev. B 72 (2005) 155106.
- [13] V. Křápek, P. Novák, J. Kuneš, D. Novoselov, D. M. Korotin, V. I. Anisimov, Phys. Rev. B 86 (2012) 195104.
- [14] P. Werner, A. J. Millis, Phys. Rev. Lett. 99 (2007) 126405.
- [15] J. Kuneš, V. Křápek, Phys. Rev. Lett. 106 (2011) 256401.
- [16] E. Pavarini, S. Biermann, A. Poteryaev, A. I. Lichtenstein, A. Georges, O. K. Andersen, Phys. Rev. Lett. 92 (2004) 176403.
- [17] J. Kuneš, V. I. Anisimov, A. V. Lukoyanov, D. Vollhardt, Phys. Rev. B 75 (2007) 165115.
- [18] H. Hafermann, K. R. Patton, P. Werner, Phys. Rev. B 85 (2012) 205106.
- [19] L. Boehnke, H. Hafermann, M. Ferrero, F. Lechermann, O. Parcollet, Phys. Rev. B 84 (2011) 075145.
- [20] X. Wang, E. Gull, L. de’ Medici, M. Capone, A. J. Millis, Phys. Rev. B 80 (2009) 045101.
- [21] M. Jarrell, J. Gubernatis, Physics Reports 269 (3) (1996) 133 – 195.
- [22] E. Gull, P. Werner, S. Fuchs, B. Surer, T. Pruschke, M. Troyer, Computer Physics Communications 182 (4) (2011) 1078 – 1082.
- [23] B. Bauer, L. D. Carr, H. G. Evertz, A. Feiguin, J. Freire, S. Fuchs, L. Gamper, J. Gukelberger, E. Gull, S. Guertler, A. Hehn, R. Igarashi, S. V. Isakov, D. Koop, P. N. Ma, P. Mates, H. Matsuo, O. Parcollet, G. Pawłowski, J. D. Picon, L. Pollet, E. Santos, V. W. Scarola, U. Schollwöck, C. Silva, B. Surer, S. Todo, S. Trebst, M. Troyer, M. L. Wall, P. Werner, S. Wessel, Journal of Statistical Mechanics: Theory and Experiment 2011 (05) (2011) P05001.

- [24] A. Albuquerque, F. Alet, P. Corboz, P. Dayal, A. Feiguin, S. Fuchs, L. Gamper, E. Gull, S. Gürtler, A. Honecker, R. Igarashi, M. Körner, A. Kozhevnikov, A. Läuchli, S. Manmana, M. Matsumoto, I. McCulloch, F. Michel, R. Noack, G. Pawłowski, L. Pollet, T. Pruschke, U. Schollwöck, S. Todo, S. Trebst, M. Troyer, P. Werner, S. Wessel, *Journal of Magnetism and Magnetic Materials* 310 (2, Part 2) (2007) 1187 – 1193.